Damage assessment of two-way RC slab subjected to blast load using mode approximation approach

[1]Xin HUANG, [2]Huirong BAO, [3]Yifei HAO[*], [3]Hong HAO

[1]Department of Naval Architecture and Ocean Engineering, School of Civil Engineering, Tianjin University, 92 Weijin Road, Nankai District, Tianjin, 300072, P. R. China
[2]China Haisum Engineering Co., Ltd., 21 Baoqing Road, Shanghai, 200031, P.R. China
[3]Tianjin University and Curtin University Joint Research Center of Structural Monitoring and Protection, School of Civil and Mechanical Engineering, Curtin University, Kent Street, Bentley, WA 6102, Australia

Abstract

Significant research efforts have been spent on studying the response and damage of structures subjected to blast loads for better life and property protections. The single-degree-of-freedom (SDOF) approach has been widely adopted to simplify the structural response analysis for engineering design purpose. However, such approach under certain circumstances oversimplifies the structural behavior and might not give reliable predictions of structural responses to blast loads. On the other hand, although detailed high fidelity finite element (FE) approach is able to give relatively accurate predictions of structural response, it is, unfortunately, not straightforward for application and very time-consuming, which impedes its application among engineers. Therefore a method that can assure not only reliability but also efficiency is highly needed for design practice. In the present study, mode approximation method with P-I diagrams is applied to analyze response and damage of RC slab due to blast load. Slab under analysis is assumed rigid-plastic and simply supported. Shear failure, bending failure and combined failure modes are considered based on different failure modes. Critical equations for structural shear and bending failures are derived respectively with appropriate failure criteria. P-I diagrams are then developed for quick damage assessments. The analytical results are verified by comparing with high fidelity numerical simulations. The reliability and efficiency of using this approach for design and analyzing RC slab response under blast loads are demonstrated.

Keywords: *Combined failure, Mode Approximation Method, P-I diagram, RC slab, blast load,*

---

[*] Corresponding author. Email: hao.yifei@outlook.com

damage assessment

1. Introduction

Detonation of explosive materials due to accidents or terrorist activities is a great threat to buildings, infrastructures and civilians. For better protection of structures, properties and lives, efficient and accurate evaluation of existing facilities and new structures in resisting blast loadings is essential. Some standards such as DoD-6055.09-STD [1] provides ways for quick assessment of structural safety under explosions based on the Q-D (quantity of explosive charge and distance to structures) criteria. However, the definition of damage levels in DoD-6055.09-STD [1] is unclear, i.e., it is not clear if the so-called damage in the standard relates to crack or collapse of infill or exterior walls, or other types of structure or structural element failure. Moreover, a structural element under blast loading might also experience different failure modes such as crush and spall failure of concrete structures, direct and diagonal shear, bending failure, etc., depending on element properties and blast loading conditions. Bending failure often occurs near center of a simply-supported structural element, while shear failure occurs close to supports. Based on experimental and analytical results, many researchers [2, 3] concluded that shear failure is highly likely to occur when a detonation is at a close-in distance from structure or when the span-to-height ratio of a structural element is relatively small.

An equivalent single-degree-of-freedom (SDOF) approach has been widely used to simplify complex behaviour of structures or structural elements for efficient analysis of structural responses subjected to blast load. Some popular structural blast designs are based on the SDOF approach [4]. Although various extensions and applications of the SDOF approach have been carried out in many cases, it is appropriate for far-field detonations in which the loading environment can be approximated by a standard shape. The SDOF approach might oversimplify a structure or a structural element due to the limitation of its mathematical form. Based on the SDOF model, shear deformation effect was either neglected in the analysis [5-7] or considered separately by another SDOF model [8, 9]. For a mixed failure mode, the SDOF model becomes invalid. Moreover, the equivalent SDOF model is derived based on the assumption of a primary structural deflection shape, which is usually taken as the counterpart under static loads, and sometimes does not reflect the true dynamic structural deflections because of inertial resistance. Sometimes the structural deflection shape in forced response phase and free-vibration phase

2

changes, which clearly is not able to be captured by a SDOF model. To obtain more reliable structural response predictions, detailed finite element (FE) model were developed for numerical simulations, e.g. [34]. Although high fidelity numerical simulations are able to give reliable predictions of structural responses, it is normally very time consuming.

The classical Mode Approximation Method (MAM) for rigid-plastic beam elements analysis has been used by many researchers. Research works have been done on different constraints and load distributions [10-12]. Comparison of results show that, Pressure-Impulse (P-I) diagrams based on rigid-plastic model have advantages in characterizing combined failure modes, with acceptable accuracy when assessing structural damage. Although rigid-plastic model neglects elastic deformation, estimated deflections by the extended MAM in most cases agree very well with the final deflections observed in tests [13], and P-I diagrams derived from a rigid-plastic model are very close to those from an elastic-to-perfectly-plastic SDOF model, especially when severe damage occurs. Ma *et al.* [14] further developed a P-I diagram method for damage assessment of structures subjected to blast load by considering both bending and shear damage. An explicit analytical solution based on the MAM for P-I diagrams was obtained which could be conveniently used for assessing structural damage. Later, Ma *et al.* [15] extended the MAM and P-I diagram method by decoupling soil-structure interaction to study underground box-shaped structure response against internal and external blast loads. The influences of nonlinear resistance-deformation relationship of materials, nonlinear soil-structure interaction parameters, and pulse shapes on P-I diagram based on the MAM were further discussed in [16-18].

Numerical and experimental studies on the response and failure of slab/plate have been done by many researchers. It has been observed that direct shear occurs near supports [19-21], and large inelastic deformation appears near center [22, 23]. Although some researchers tried to represent the slab response by an SDOF system [24], more results show that the combined failure appears under certain circumstances for both square and circular plates [25, 26]. However, the analytical solution based on MAM approach cannot be found yet in open literature. Theoretically using a beam element with MAM approach would not cause big errors in estimating the maximum deflection when the aspect ratio (ratio of long to short edge $\eta = L_a / L_b$, where L_a and L_b are lengths of long and short edge respectively) of a slab is larger than 2.0 because the slab with large aspect ratio is normally considered as a one-way slab. Correspondingly its response is

basically the same as a beam. When the aspect ratio is between 1.0 and 2.0, P-I diagram results will change since the length of structural element used in governing equations may adopt either shorter or longer edge. Therefore the MAM developed for beam or one-way slab may not lead to accurate predictions of responses of two-way slabs. The present study extended the MAM from beam element to two-way slab, aiming to develop a reliable and efficient analytical approach for design and analysis of protective structures subjected to blast load. To verify the results for different failure modes, high fidelity numerical simulations with validated numerical models are carried out on some special cases. A case study is given at the end of the present paper.

2. Failure criteria and modes

The present study focuses on four-side simply-supported slabs. According to the previous results obtained by other researchers [2, 3] for simply supported or clamped beams, the ratio of centerline-deflection to half-span is used to define the flexural damage levels since the largest ductile plastic deformation usually appears at the beam center due to bending response. The average shear strain is defined as shear damage levels since the shear plastic deformation usually appears near the supports, as shown in Fig. 1.
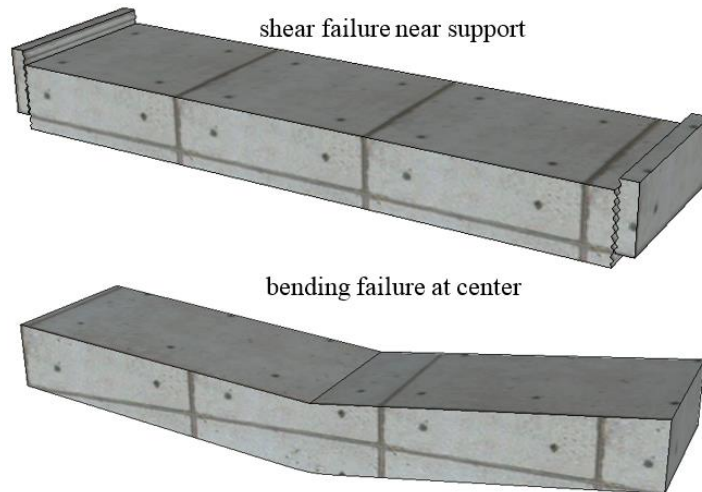

Fig. 1 Sketch of shear and bending failure mode

If a strip is taken at center of a slab to represent the maximum displacement caused by shear/bending force, its failure profile is the same as that of a beam. This has been adopted by civil engineers in design practice with respect to two-way RC slabs to simplify the design calculation. Therefore the maximum transverse displacement due to bending and direct shear

failure near supports in the present study can be expressed as follows according to results of Yu and Jones [2], Li and Jones [12], and Bai and Johnson [27]:

$$z_m = L\beta_0 \quad and \quad z_s = \gamma_v \delta h \tag{1}$$

where z_m is the maximum transverse displacement due to bending, L is the half edge length in different failure modes, β_0 is the ratio of centerline deflection to half span, z_s is the maximum transverse displacement due to direct shear, γ_v is the average shear strain in unit length, δ is the half-width of the shear band obtained from experimental results, h is the thickness of slab. In the present study, δ is defined as 0.866 according to [28]. Table 1 shows different damage levels under empirical bending and shear failure criteria used in [14].

Table 1 Different damage level under empirical bending and shear failure criteria

Failure type	Criteria	Light Damage (%)	Moderate Damage (%)	Severe Damage (%)
Shear	Average shear strain	1	2	3
Bending	Ratio of centerline deflection to half span	2.5	6	12.5

Pulse shape of blast load can be of many forms, e.g. rectangular, triangular, and parabolic. Pulse shape effect on the structural behavior has been discussed by many researchers, e.g., Youngdahl [29], Youngdahl [30], Li and Meng [31], Li and Jones [32], and the differences in responses obtained with different pulse shapes can be estimated though analytical results reported by Huang *et al.* [17]. In the present study, a triangular pulse load is used. As shown in Fig. 2, the triangular pulse load can be defined by the peak reflected pressure p_o, with equivalent duration t_d calculated based on impulse. The pressure acting on slab can be expressed as:
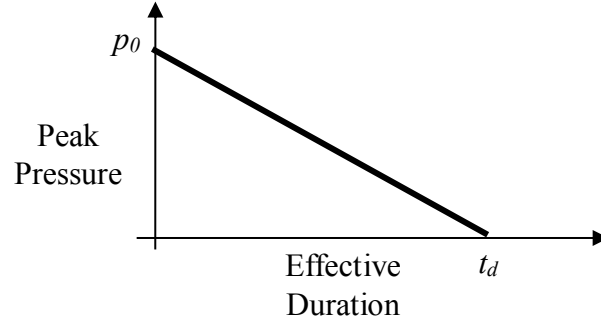
$$p = p_0 \left(1 - \frac{t}{t_d} \right) \tag{2}$$

Fig. 2 Triangular pulse load
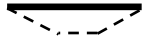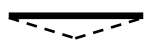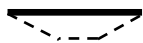
Similar to the analysis for beam element, there are several possible transverse velocity profiles which include pure shear failure mode, pure bending failure modes, and combined failure modes. A dimensionless strength ratio is introduced as below [14].

$$\nu = \frac{Q_0 L_a}{2M_0} \tag{3}$$

where Q_0 and M_0 are respectively the shear and bending strength of slab, L_a is the length for longer edge of slab.

Table 2 shows the velocity profiles of different phases under different failure modes. Such profiles make it possible to consider different failure modes at the same time. Moreover, as judgment of failure only involves peak reflected pressure and dimensionless strength ratio of slab, it is convenient t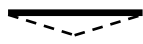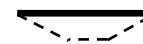o use alternate velocity profiles to judge initiations of different failure modes, and response calculation can be carried out accordingly. Besides the numbers 1-5 that are used to distinguish the failure modes, sub-letters a and b are adopted to represent the case with failure along long or short edge, respectively. Coordinate of analysis model is defined in Fig. 3 in which the origin of coordinate system is at the centroid of slab. Failure profiles for each mode are shown in Fig. 4. Mode 1 contains pure shear failure that includes sub-mode 1a and sub-mode 1b. Mode 2 is for simple bending failures with a plastic hinge at the center of the element, and this failure mode has two sub-modes named sub-mode 2a and sub-mode 2b. Mode 3, divided into sub-mode 3aa, sub-mode 3ab, sub-mode 3ba and sub-mode 3bb, can be considered as combinations of mode 1 and mode 2. Mode 4 is the complex bending failure mode which has a plastic zone at the middle of the element. Similar to mode 2, mode 4 is divided into sub-mode 4a and sub-mode 4b. Mode 5 contains combinations of mode 1 and mode 4, including pre-defined sub-mode 5aa, sub-mode 5ab, sub-mode 5ba, and sub-mode 5bb, as shown in Figure 4.

Table 2 Velocity profile

	Mode 1	Mode 2	Mode 3	Mode 4	Mode 5
Phase 1					
Phase 2					
Phase 3	N.A.	N.A.			
Phase 4	N.A.	N.A.	N.A.	N.A.	

Fig. 3 Coordinate of analysis model

sub-mode 1a sub-mode 1b

sub-mode 2a sub-mode 2b

sub-mode 3aa sub-mode 3ab

sub-mode 3ba sub-mode 3bb

sub-mode 4a sub-mode 4b

sub-mode 5aa sub-mode 5ab
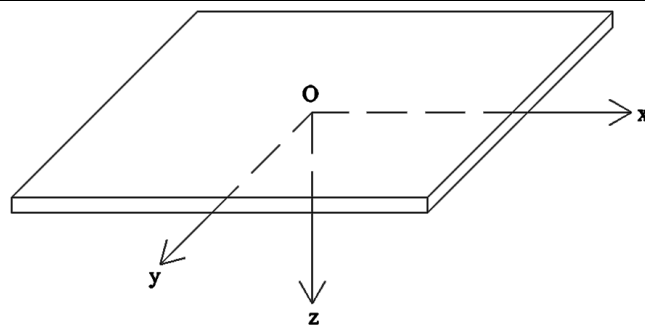
sub-mode 5ba sub-mode 5bb

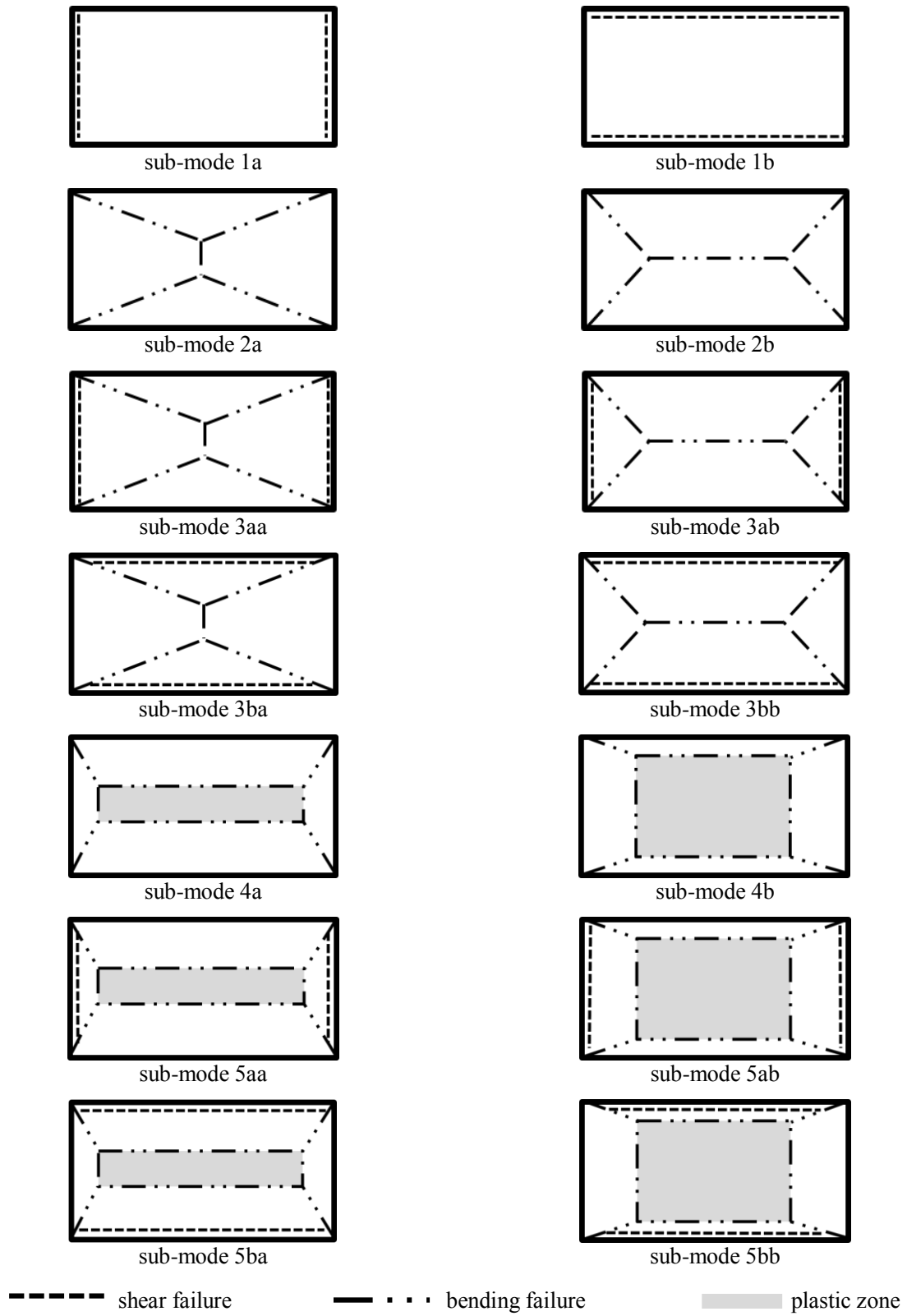- - - - shear failure — · · · bending failure ▨ plastic zone

Fig. 4 Failure profile of sub-modes

Derivation of structural final displacements for different sub-modes is summarized as follows. The boundary conditions are assumed not to change for the transition from one phase to another of a specified failure mode and damping is neglected. The final displacement and velocity of slab at the end of a particular phase are always used as the initial conditions in the following phase if applicable.

Mode 1: pure shear failure

Sub-Mode 1a: pure shear failure along the short edge.

Shear failure mode describes the direct shear failure occurring at two supports along the short edges that carry the maximum shear force in x-axis direction. The deformation due to bending is ignored in this mode. There are totally two phases in this mode including a loading phase (phase 1) and a post-loading phase (phase 2) which are assumed to end at t_d and t_f, respectively.

The governing equation for phase 1 is

$$\frac{\partial Q}{\partial x} = -p + m\ddot{z}_s \tag{4}$$

where Q is the transverse shear force in slab, p_0 is the uniformed force acting on slab, m is the unit mass of slab, $\ddot{z}_s$ is the acceleration due to shear force.

Boundary and initial conditions are

$$Q(x=0)=0, \quad Q(x=L_a)=-Q_0 \tag{5}$$

$$\dot{z}_s(t=0)=0, \quad z_s(t=0)=0 \tag{6}$$

where $\dot{z}_s$ and z_s are velocity and displacement due to shear force respectively, t is the time variable.

By integrating Eq.(4) with respect to time, at the end of phase 1 when $t=t_d$, the maximum slab displacement $z_s(t_d)$ and velocity of $\dot{z}_s(t_d)$ are solved.

In phase 2, the governing equation becomes

$$\frac{\partial Q}{\partial x} = m\ddot{z}_s \tag{7}$$

Motion termination time t_f of phase 2 is determined when $\dot{z}_s = 0$. Final transverse maximum displacement of slab due to shear is derived as

$$z_s\left(t_f\right) = \frac{p_0 t_d^2 \left(p_0 L_a - Q_0\right)}{2 m Q_0} \tag{8}$$

Sub-Mode 1b: pure shear failure along the long edge.

The equations and derivation are similar to mode 1a, but x-axis changes to y-axis. The governing equation for phase 1 changes to

$$\frac{\partial Q}{\partial y} = -p + m\ddot{z}_s \tag{9}$$

The governing equation for phase 2 changes accordingly, and L_a is replaced by L_b in the derivation which means the length of shorter edge of slab. The final structural maximum displacement is

$$z_s\left(t_f\right) = \frac{p_0 t_d^2 \left(p_0 L_b - Q_0\right)}{2 m Q_0} \tag{10}$$

Mode 2: simple bending failure (1 hinge)

Sub-Mode 2a: simple bending failure along the long edge.

There are also two phases in this mode including a loading phase (phase 1) and a post-loading phase (phase 2) which end at t_d and t_f respectively. In phase 1, the governing equation is

$$\frac{\partial Q}{\partial x} = -p + m\ddot{z}_m\left(1 - \frac{x}{L_a}\right) \tag{11}$$

where $\ddot{z}_m$ is the acceleration due to bending moment.

Boundary and initial conditions are

$$Q(x=0) = 0, \quad Q(x=L_a) = -Q_0, \quad M(x=0) = M_0, \quad M(x=L_a) = 0 \tag{12}$$

$$\dot{z}_m(t=0) = 0, \quad z_m(t=0) = 0 \tag{13}$$

where M is the bending moment in slab, $\dot{z}_m$ and z_m are velocity and displacement due to bending moment, respectively.

In phase 2, the governing equation changes to

$$\frac{\partial Q}{\partial x} = m\ddot{z}_m \left(1 - \frac{x}{L_a}\right) \tag{14}$$

The final time t_f of phase 2 can be determined with the condition $\dot{z}_m = 0$. The final maximum bending displacement is then derived as

$$z_m(t_f) = \frac{3p_0 t_d^2 \left(p_0 L_a^2 - 2M_0\right)}{8mM_0} \tag{15}$$

Sub-Mode 2b: simple bending failure along the short edge

Equations and derivation are similar to mode 1a. The governing equation for phase 1 changes to

$$\frac{\partial Q}{\partial y} = -p + m\ddot{z}_m \left(1 - \frac{y}{L_b}\right) \tag{16}$$

and the governing equation for phase 2 also changes accordingly. The final maximum bending displacement at slab center is

$$z_m(t_f) = \frac{3p_0 t_d^2 \left(p_0 L_b^2 - 2M_0\right)}{8mM_0} \tag{17}$$

Mode 3: combined shear and simple bending failure

Sub-Mode 3aa: combined failure mode, shear failure along the short edge and simple bending failure along the long edge

Mode 3aa is the combination of mode 1a and mode 2a when both shear failure and bending failure occur in the slab. Shear failure occurs at two supports while bending failure induces plastic hinge at the center of the slab. Deformation of slab includes one loading phase (phase 1) and two post-loading phases (phase 2 and phase 3) which are assumed to end at t_d, t_s, and t_f respectively.

In phase 1, the governing equation is given by

$$\frac{\partial Q}{\partial x} = -p + m\ddot{z}_s + m\left(\ddot{z}_m - \ddot{z}_s\right)\left(1 - \frac{x}{L_a}\right) \tag{18}$$

with the same boundary and initial conditions given in Eqs.(6), (12), and (13).

Similar to mode 1a and mode 2a, at the end of phase 1 when $t = t_d$ the maximum displacement and velocity of the element due to shear and bending deformation can be determined as $z_s(t_d)$, $\dot{z}_s(t_d)$, $z_m(t_d)$, and $\dot{z}_m(t_d)$ respectively.

In phase 2, the governing equation is

$$\frac{\partial Q}{\partial x} = m\ddot{z}_s + m(\ddot{z}_m - \ddot{z}_s)\left(1 - \frac{x}{L_a}\right) \tag{19}$$

Solving Eq.(19), at the end of phase 2 when $\dot{z}_s(t_s) = 0$, displacement due to shear stops, while bending displacement remains to the next phase of motion. The maximum displacement associated to the shear mode is derived as below, and the maximum displacement and velocity due to bending motion can then be solved as

$$z_s(t_s) = \frac{p_0 t_d^2 \left(4Q_0 L_a - p_0 L_a^2 - 6M_0\right)}{4m(3M_0 - 2Q_0 L_a)} \tag{20}$$

In phase 3, only response related to the bending failure mode remains, and the governing equation is the same as Eq.(14). Similarly, when motion terminates the final displacement is determined as

$$z_m(t_f) = \frac{p_0 t_d^2 \left(5p_0 L_a^2 M_0 + 4Q_0 L_a M_0 - 3p_0 L_a^3 Q_0 - 6M_0^2\right)}{4mM_0(3M_0 - 2Q_0 L_a)} \tag{21}$$

Sub-Mode 3ab: combined failure mode, both shear and bending failure along the short edge

Equations and derivation are again similar to mode 3aa. The governing equations for phase 1 change to

$$\frac{\partial Q}{\partial y} = -p + m\ddot{z}_s + m(\ddot{z}_m - \ddot{z}_s)\left(1 - \frac{y}{L_b}\right)$$
$$\frac{\partial Q}{\partial x} = -p + m\ddot{z}_s \tag{22}$$

The governing equations for phase 2 and phase 3 change accordingly, and the final structural deflections are

$$z_s(t_s) = \frac{p_0 t_d^2 \left(p_0 L_a - Q_0\right)}{2mQ_0} \tag{23}$$

$$z_m\left(t_f\right)=\frac{p_0 t_d^2\left(3p_0 L_b^2 Q_0-2p_0 L_a M_0-4M_0 Q_0\right)}{8mM_0 Q_0} \tag{24}$$

Sub-Mode 3ba: combined failure mode, both shear and bending failure along the long edge

Equations and derivation are similar to mode 3ab, but x coordinate is swapped with y coordinate. The governing equations for phase 1 change to

$$\frac{\partial Q}{\partial x}=-p+m\ddot{z}_s+m\left(\ddot{z}_m-\ddot{z}_s\right)\left(1-\frac{x}{L_a}\right)$$
$$\frac{\partial Q}{\partial y}=-p+m\ddot{z}_s \tag{25}$$

and the governing equations for phase 2 and phase 3 change accordingly. The final structural deflections are

$$z_s\left(t_s\right)=\frac{p_0 t_d^2\left(p_0 L_b-Q_0\right)}{2mQ_0} \tag{26}$$

$$z_m\left(t_f\right)=\frac{p_0 t_d^2\left(3p_0 L_a^2 Q_0-2p_0 L_b M_0-4M_0 Q_0\right)}{8mM_0 Q_0} \tag{27}$$

Sub-Mode 3bb: combined failure mode, shear failure along the long edge and simple bending failure along the short edge

Equations and derivation are similar to mode 3aa, but x and y coordinates are swapped. The governing equation for phase 1 change to

$$\frac{\partial Q}{\partial y}=-p+m\ddot{z}_s+m\left(\ddot{z}_m-\ddot{z}_s\right)\left(1-\frac{y}{L_b}\right) \tag{28}$$

and the governing equations for phase 2 and phase 3 change accordingly, and the final structural deflections are

$$z_s\left(t_s\right)=\frac{p_0 t_d^2\left(4Q_0 L_b-p_0 L_b^2-6M_0\right)}{4m\left(3M_0-2Q_0 L_b\right)} \tag{29}$$

$$z_m\left(t_f\right)=\frac{p_0 t_d^2\left(5p_0 L_b^2 M_0+4Q_0 L_b M_0-3p_0 L_b^3 Q_0-6M_0^2\right)}{4mM_0\left(3M_0-2Q_0 L_b\right)} \tag{30}$$

Mode 4: complex bending failure (plastic zone at center with 2 plastic hinges)
Sub-Mode 4a: complex bending failure along the long edge

Bending failure with a plateau deformation at the central portion of the slab may occur when blast load is sufficiently intensive. Being different from mode 2a, in this mode, two plastic hinges are generated offset from center of the slab. Three phases including one loading phase (phase 1) and two post-loading phases (phase 2 and phase 3) which end at t_d, t_1, and t_f, respectively are considered.

In phase 1, the governing equation is expressed as

$$\frac{\partial Q}{\partial x} = -p + m\ddot{z}_m \left(\frac{L_a - x}{L_a - \xi_0} \right) \tag{31}$$

where ξ_0 is the distance of plastic hinge from the slab center.

Initial conditions are the same as Eqs.(6) and (13). Boundary conditions are as follows

$$Q(x = \xi_0) = 0, \quad Q(x = L_a) = -Q_0, \quad M(x = \xi_0) = M_0, \quad M(x = L_a) = 0 \tag{32}$$

At the end of loading period, when $t = t_d$, the plastic hinge location indicated by ξ_0 is derived as

$$\xi_0 = L_a - \sqrt{\frac{6M_0}{p_0}} \tag{33}$$

In phase 2, the action of blast load has been end, and the velocity profile is the same as that in phase 1. However, the two plastic hinges start to move toward the center of slab. At the end of phase 2, the two plastic hinges meet at slab center and phase 3 motion then starts. The governing equation of phase 2 motion is

$$\frac{\partial Q}{\partial x} = m\ddot{z}_m \left(\frac{L_a - x}{L_a - \xi_0} \right) \tag{34}$$

In phase 3, the governing equation is the same as Eq.(14) and it can be solved in a similar way as for mode 2a.

At the end of phase 3 when $t = t_f$, slab motion stops and the final bending displacement at slab center is given by

$$z_m(t_f) = \frac{p_0 t_d^2 \left(2 p_0 L_a^2 - 3M_0 \right)}{6mM_0} \tag{35}$$

Sub-Mode 4b: complex bending failure along the short edge

Equations and derivation are similar to mode 4a, but x coordinate is replaced by y coordinate. The governing equation for phase 1 changes to

$$\frac{\partial Q}{\partial y} = -p + m\ddot{z}_m\left(\frac{L_b - x}{L_b - \xi_0}\right) \tag{36}$$

Half width of plastic zone is derived as

$$\xi_0 = L_b - \sqrt{\frac{6M_0}{p_0}} \tag{37}$$

The governing equations for phase 2 and phase 3 change accordingly, and the final maximum structural displacement is

$$z_m\left(t_f\right) = \frac{p_0 t_d^2\left(2p_0 L_b^2 - 3M_0\right)}{6mM_0} \tag{38}$$

Mode 5: combined shear and complex bending failure

Sub-Mode 5aa: combined failure mode, shear failure along the short edge and complex bending failure along the long edge

Mode 5 is the most complicated mode which combines mode 1 and mode 4. There are altogether four phases including one loading phase (phase 1) and three post-loading phases (phase 2, phase 3, and phase 4). They are assumed to end at t_d, t_s, t_l and t_f, respectively.

In phase 1, both the shear and bending deformation occur. The governing equation is

$$\frac{\partial Q}{\partial x} = -p + m\ddot{z}_s + m\left(\ddot{z}_m - \ddot{z}_s\right)\left(\frac{L_a - x}{L_a - \xi_0}\right) \tag{39}$$

Boundary conditions are the same as Eq.(32), and initial conditions can be obtained from Eqs.(6) and (13).

At the end of phase 1, half width of plastic zone is

$$\xi_0 = L_a - \frac{3M_0}{Q_0} \tag{40}$$

In phase 2, velocity profile is the same as that in phase 1, while shear deformation tends to stop. The governing equation becomes

$$\frac{\partial Q}{\partial x} = m\ddot{z}_s + m\left(\ddot{z}_m - \ddot{z}_s\right)\left(\frac{L_a - x}{L_a - \xi_0}\right) \tag{41}$$

At the end of phase 2 when $t = t_s$, shear deformation stops. The final maximum shear displacement of phase 2 is given by

$$z_s(t_s) = \frac{p_0 t_d^2 (3p_0 M_0 - 2Q_0^2)}{4mQ_0^2} \tag{42}$$

In phase 3, the two plastic hinges start to move toward center of the slab. The governing equation is the same as Eq.(34). Similarly, at the end of phase 3, when $t = t_1$, the two plastic hinges coincide at the slab center.

In phase 4, the governing equation is the same as Eq.(14). Finally the maximum bending displacement is

$$z_m(t_f) = \frac{p_0 t_d^2 (2p_0 L_a^2 - 3M_0)}{6mM_0} \tag{43}$$

Sub-Mode 5ab: combined failure mode, both the shear failure and complex bending failure along the short edge

The governing equations for phase 1 change to Eq.(4) and

$$\frac{\partial Q}{\partial y} = -p + m\ddot{z}_s + m(\ddot{z}_m - \ddot{z}_s)\left(\frac{L_b - y}{L_b - \xi_0}\right) \tag{44}$$

Half width of plastic zone is derived as

$$\xi_0 = L_b - \sqrt{\frac{6L_a M_0}{Q_0}} \tag{45}$$

The governing equations for phase 2, 3 and 4 change accordingly, and the final maximum structural displacements are

$$z_s(t_s) = \frac{p_0 t_d^2 (p_0 L_a - Q_0)}{2mQ_0} \tag{46}$$

$$z_m(t_f) = \frac{p_0 t_d^2 (p_0 L_b^2 - 3M_0)}{6mM_0} \tag{47}$$

Sub-Mode 5ba: combined failure mode, both shear failure and complex bending failure along the long edge

The governing equations for phase 1 change to Eqs.(9) and (39). Half width of plastic zone is derived as

$$\xi_0 = L_a - \sqrt{\frac{6L_b M_0}{Q_0}} \tag{48}$$

The governing equations for phase 2, 3 and 4 change accordingly, and the final maximum structural displacements are

$$z_s(t_s) = \frac{p_0 t_d^2 (p_0 L_b - Q_0)}{2mQ_0} \tag{49}$$

$$z_m(t_f) = \frac{p_0 t_d^2 (p_0 L_a^2 - 3M_0)}{6mM_0} \tag{50}$$

Sub-Mode 5bb: combined failure mode, shear failure along the long edge and complex bending failure along the short edge

The governing equation for phase 1 changes to Eq.(44). Half width of plastic zone is derived as

$$\xi_0 = L_b - \frac{3M_0}{Q_0} \tag{51}$$

The governing equations for phase 2, 3 and 4 change accordingly, and the final maximum displacements are as Eq.(42) and

$$z_m(t_f) = \frac{p_0 t_d^2 (p_0 L_b^2 - 3M_0)}{6mM_0} \tag{52}$$

3. P-I diagrams and discussions

In each sub-mode discussed in the above section, the final shear displacement z_s for direct shear failure, the final bending displacement z_m for bending failure, or both for combined failure are derived. Given certain failure criteria in terms of the maximum shear and bending displacements, P-I diagrams for different sub-modes then can be obtained. Similar to the work done by Ma *et al.* [14], in the present study, two normalized variables *P** and *I** of blast load are defined as:

$$P^* = \frac{p_0}{(Q_0/L_a)} \quad and \quad I^* = \frac{p_0 t_d}{\sqrt{2mQ_0}} \tag{53}$$

From equations for final displacements induced by shear and bending failure, P-I diagrams can be represented in unified forms as

$$S\left(P^*, I^*\right) = \delta \cdot h \cdot \gamma_v \quad and \quad B\left(P^*, I^*\right) = L_a \cdot \beta \tag{54}$$

where the shear and bending failure criteria given respectively in Eq.(1) are used.

$S\left(P^*, I^*\right)$ and $B\left(P^*, I^*\right)$ are implicit expressions and equal to the final shear and bending displacement respectively.

3.1   Distribution of failure modes

By determining the relevant parameters, P-I diagrams can be plotted for all sub-modes. The difference of sub-modes depends on peak reflected pressure p_0, dimensionless strength ratio v, and aspect ratio of slab η.

Some general observations of structural responses as outlined below are used to judge the failure mode:

1) in phase 1 (loading phase) of every mode, the structural acceleration induced by shear force or bending moment should be positive;

2) in a post-loading phase, the structural acceleration should be negative;

3) distance between plastic hinge and the slab center (ξ_0) in modes 4 and 5 should be larger than zero;

4) the maximum bending moment should be smaller than the bending strength of slab in pure shear mode, and vice versa in pure bending mode.

Judgment of slab failure sub-mode can be divided into two steps. The first step is to decide its failure mode according to Fig. 5, in which the half-span length L in initial conditions used in flowchart is temporarily defined as L_a. The second step is to decide its sub-mode by substituting L_a and L_b to expressions of structural accelerations, i.e. $\ddot{z}_s$ and $\ddot{z}_m$, respectively, that can be obtained by solving the governing equations in phase 1 if applicable. If both L_a and L_b make the acceleration(s) larger than zero, shear failure will occur along the long edge and bending failure will occur along the short edge if applicable. If only L_a makes structural acceleration(s) smaller than zero, shear failure will appear along the short edge and bending failure will occur along the

18

long edge if applicable. For example, assuming a slab will fail in mode 3, when L_a and L_b make $\ddot{z}_s$ in phase 1 larger than zero while only L_a can make $\ddot{z}_m$ larger than zero, the sub-mode would be sub-mode 3ba.
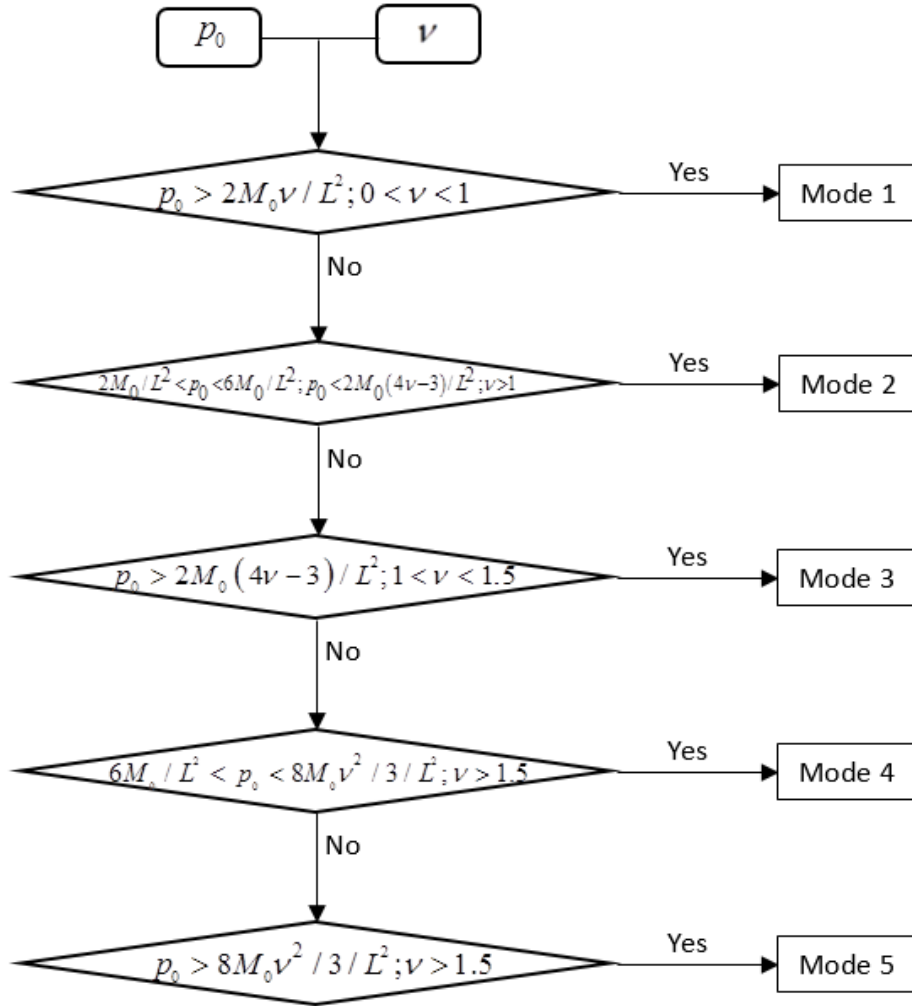

Fig. 5 Failure mode judging flowchart

3.2 Model validation

From Eqs.(53) and (54), P-I diagrams based on the MAM approach can be obtained for slabs. To validate the analytical solutions derived above, numerical simulations are carried out using commercial code ANSYS-AUTODYN. The obtained structural responses with derived P-I diagrams from numerical simulations are compared to those obtained from analytical solutions.

3.2.1 Material model, mesh convergence tests and model validation

Before comparing the numerical simulation results with analytical predictions, the accuracy of numerical model is validated by simulating a field blasting tests. In the blast tests reported by Jones *et al.* [33], 2000×1000×100 mm^3 RC slabs were tested. Both tensile and compressive faces of the RC slab were reinforced with ϕ12 mm steel bars with 100 mm interval along the long edge and ϕ12 mm steel bars with 200 mm interval along the short edge. The yield stress and Young's modulus of the reinforcement are 600 MPa and 200 GPa, respectively. The static strengths of concrete are 39.5 MPa in compression and 8.2 MPa in tension. The short edges of RC slab were clamped while the other edges were set free. The RC slabs were tested under free field explosion with scaled distances of 3.0, 1.5 and 0.93 m/kg$^{1/3}$, respectively. The construction details of the RC slabs are shown in Fig. 6. Numerical model and loadings according to experimental set-up are developed to simulate those tests.
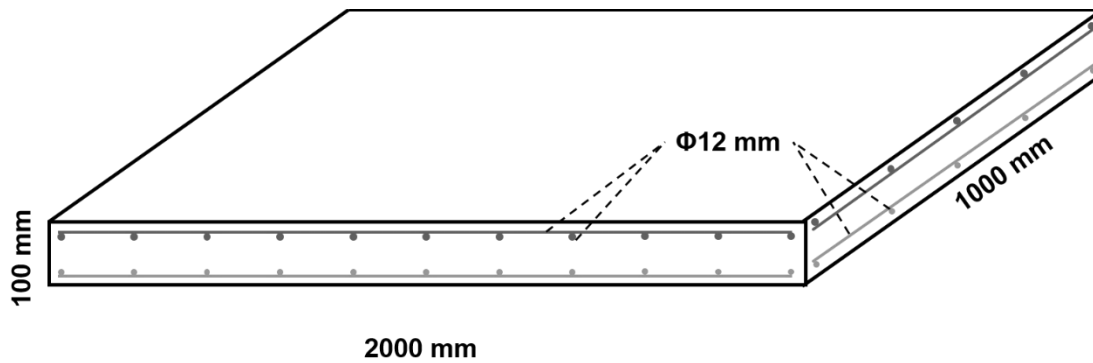

Fig. 6 Rebar arrangement of the RC slab tested by [33] (not to scale)

In the present study, the material models used for concrete and reinforcing steel are RHT model and Johnson-Cook model, respectively. Both of the models are available in the AUTODYN material library database. Parameters for concrete and steel in the respective models are the same as those used in the tests as listed in Table 3.

Table 3. List of parameters of material models

Parameter	RHT concrete model	Parameter	Johnson-Cook steel model
Reference density	ρ=2.75 g/cm^3	Reference density	ρ=7.83 g/cm^3
Shear modulus	G=11.79 GPa	Shear modulus	G=81.8 GPa
Compressive strength	f_c=39.5 MPa	Yield stress	σ_y=600 MPa
Tensile strength	f_t/f_c=0.2076	Hardening constant	B=510 MPa
Shear strength	f_s/f_c=0.18	Hardening exponent	n=0.26
Compressive strain rate exponent	α=0.032	Strain rate constant	C=0.014
Tensile strain rate exponent	δ=0.036	Thermal softening exponent	m=1.03
		Melting temperature	T_{melt}=1793 K

In the numerical simulation, the blast load is obtained from UFC-3-340-02 [4] and applied on 3-D RC slab model directly. The numerical models of 2000×1000×100 mm^3 RC slab are built according to the descriptions in Jones *et al.* [33]. For mesh convergence test, a few models with different mesh sizes are built and a typical one is illustrated in Fig. 7. Considering computational cost and due to symmetry of the slab, only half of the slab is modelled. Simulation with scaled distance of 3.0 m/kg$^{1/3}$ is carried out first. The aim of mesh convergence study is to find a proper mesh size which suitable for calculation and the possible shortest calculating time. The concrete material is considered as homogeneous for simplification, and an RHT model is adopted to minimize such material simplification. Four mesh sizes for concrete, which is modelled by solid elements, i.e. 32×32×24 mm^3, 16×16×12 mm^3, 8×8×6 mm^3 and 4×4×3 mm^3, respectively, are considered. The rebars are modelled by beam elements with element sizes of 32 mm, 16 mm, 8 mm, and 4 mm accordingly. The two parts, namely concrete and rebars, are joined in AUTODYN automatically by the "join" command so that the concrete and reinforcement bars are assumed to be perfectly bonded. The numerically simulated time histories of deflections at the RC slab center with different mesh sizes are plotted and compared with that recorded in the test in Fig. 8. It can be seen that simulations with solid element sizes of 4×4×3 mm^3 and 8×8×6 mm^3 for concrete and beam elements of 4 mm and 8 mm for rebars give similar structural response prediction, and the results agree well with the test data. It can also be observed in Fig. 8 that although increasing the element size can reduce the element number and save the computational time, it cannot give accurate prediction of the structural response. To optimize the

effects of computational time and calculation accuracy, solid element size of $8\times8\times6$ mm^3 for concrete and beam element size of 8 mm for rebars are adopted in the subsequent simulations.
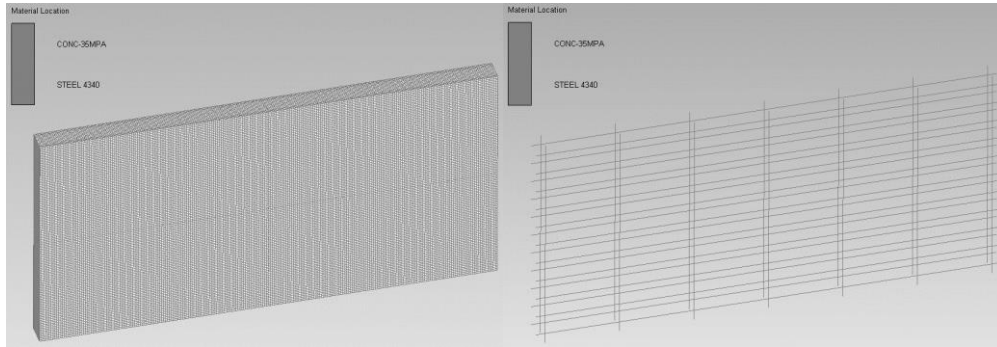
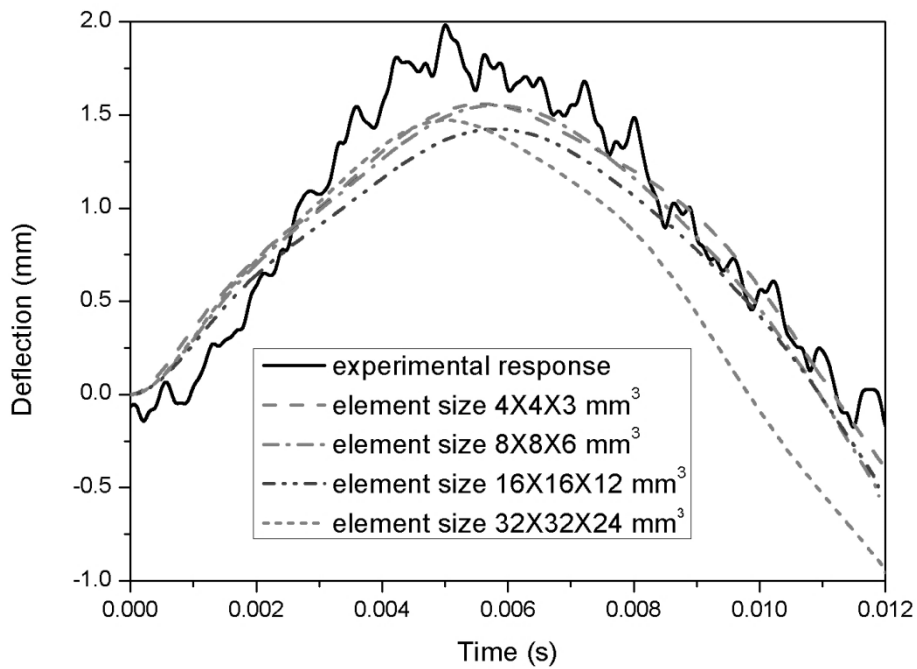

Fig. 7 3-D model of RC wall and rebar mesh

Fig. 8 Comparisons of numerical simulation results with testing data

To further validate the numerical model, simulation of the RC slab under blast loading with the scaled distance of 1.5 m/kg$^{1/3}$ is also carried out, and the simulation result is given in Fig. 9. Although the deflection time history was not given in the paper by Jones *et al.* [33], the authors stated that the maximum deflection was 7.9 mm. Given the numerical prediction of the maximum deflection of 6.9 mm, the difference is only 1 mm with error of -12.6%, indicating that the numerical model gives reasonable predictions of RC slab responses under blast loads.
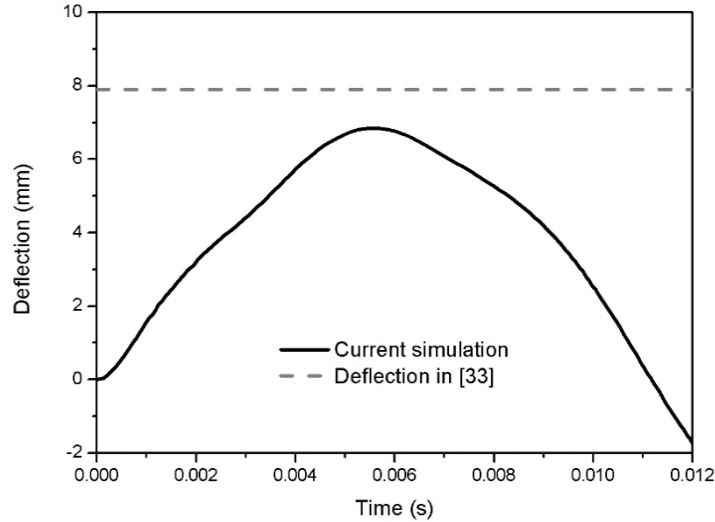
Fig. 9 Numerically predicted structural deflection time history versus maximum deflection given in [33]

3.2.2 Comparison of numerical and analytical results

The validated numerical model is used to verify the proposed analytical model in this section. An RC slab with dimension of 3050×2440×115 mm³ (accordingly the aspect ratio of 1.25) under free air blast load is employed. The boundary condition for the four sides of the slab is assumed simply supported. Considering computational cost and due to symmetry of the slab, only one quarter of the full slab is modelled and simulated. The full model of the RC wall and the arrangement of rebars are similar to those in Fig. 7. Solid elements of size 8×8×6 mm³ are used to model concrete and 8 mm beam elements are used to model rebars, as described above according to the mesh convergence test. The total numbers for solid and beam elements are 557180 and 3160, respectively.

Three series of numerical simulations are carried out and the method to obtain numerical P-I curves consists of four stages. In the first stage, three blast loads, which are estimated to cause light, moderate, and severe damages, respectively, in the RC slab, are obtained from final structural displacement equations in MAM approach. Secondly, the above three blast loads are used in numerical simulations to obtain the structural responses corresponding to the shear and bending damage for the three damage levels. The total simulation time is set as 300 ms to make sure that the peak structural response is captured and the model is in free-vibration phase. The average residual displacement values in the free vibration phase are considered as the permanent

23

displacements caused by shear and bending damage, respectively, and are set as reference for defining the damage in the following simulations. Thirdly, blast loads with different combinations of pressures and durations are used as input to calculate slab responses. The values of the input pressure and impulse are adjusted to assure that the errors between the simulated structural responses and the reference responses established in stage 2 are less than 5% for accepting the slab having the same level of damage as the reference case. Repeating this process, a series of P-I data points corresponding to the same slab damage level can be obtained. Lastly, the obtained pressure and impulse data points are connected by discrete Bezier splines to form the numerical P-I curves.

Results from the numerical simulations are then compared with those from analytical solutions. Shear resistance of unit RC wall strip is calculated as 183.95 KN, and its bending resistance is 153.3 KN·m. Accordingly, the dimensionless strength ratio defined in Eq.(3) is 1.19. The failure pattern of the slab is sub-mode 3aa according to the guides mentioned in Section 3.1 for judging the slab failure sub-mode.
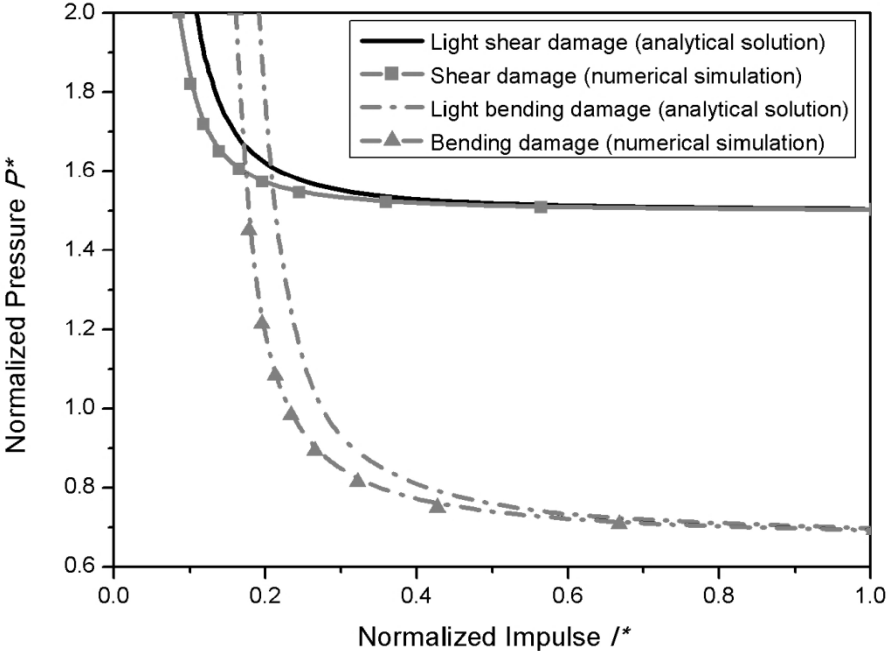
a) Light bending damage and moderate shear damage
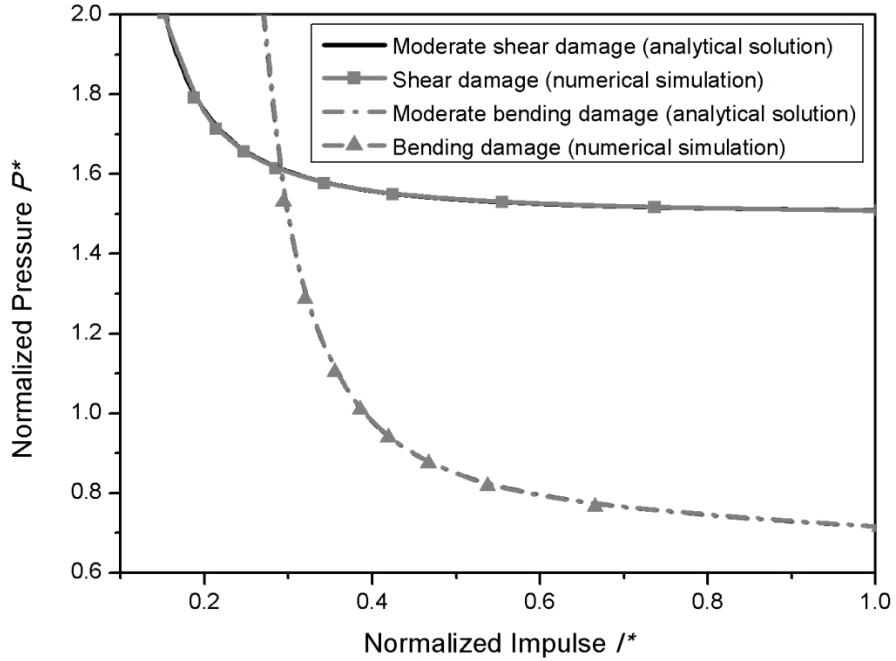
b) Moderate bending damage and severe shear damage
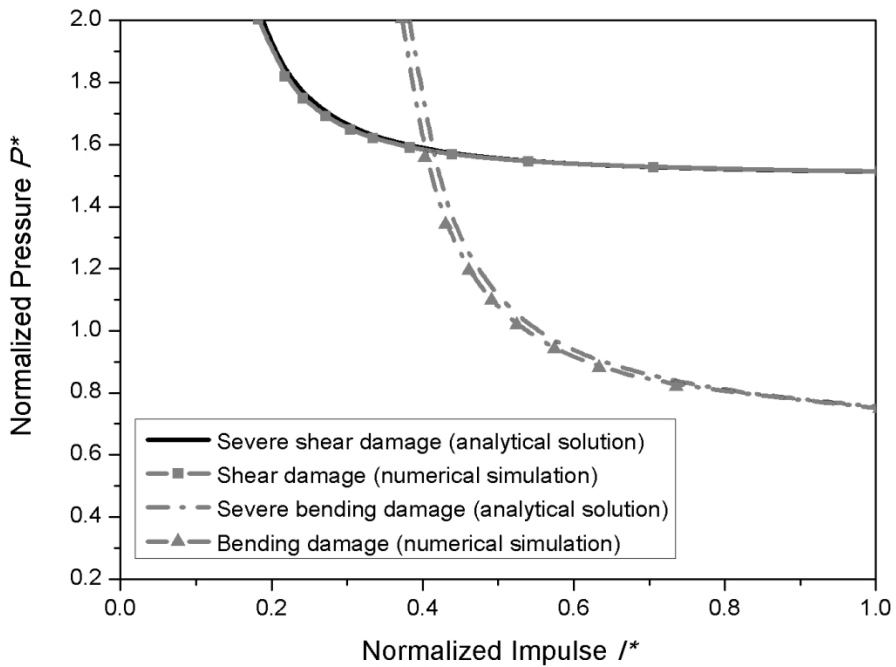
c) Severe bending damage and severe shear damage

Fig. 10 Comparisons of analytical and numerical P-I diagrams of the example slab corresponding to the three damage levels

Fig. 10 compares the analytical and numerical derived P-I curves. The P-I curves based on numerical simulations normally locates at the lower left side of those from MAM approach, indicating the above derived analytical predictions based on MAM approach slightly underestimate the RC wall damage to blast load or over predict the wall blast loading resistance capacity. In scenarios corresponding to the moderate and severe damages as shown in Fig. 10b and Fig. 10c, shear and bending damages generated from the analytical solution and numerical simulation agree very well. However, errors of the P-I diagrams for both the shear and bending damage in low damage case (Fig. 10a) becomes considerable, especially in the impulsive and dynamic regions of the P-I diagram. The relatively prominent error in light damage level may be attributed to neglecting the elastic response of the wall in MAM approach. Under moderate to severe damage condition, the plastic deformation of the slab is significant and neglecting the small elastic deformation introduces only insignificant error. On the other hand, under light damage condition, the plastic deformation might be comparable to the elastic deformation in the numerical simulation. Neglecting elastic deformation in MAM approach therefore introduces relatively large errors. Nonetheless, the above comparisons demonstrate that the derived analytical solutions give good RC slab response predictions.

3.3   Further discussions

The aspect ratio η affects the distribution of failure modes. For example, when η is close to 1.0, initial condition of sub-mode 1a is approximately the same as sub-mode 1b, therefore the two sub-modes become similar/identical. For another instance, when η is large enough (larger than 2.0 based on the current analysis and engineering experience), shear failure will probably appear along the long edge and bending failure appears along the short edge. When η is between 1.0 and 2.0, distribution of the sub-modes is complex. Some of initial conditions for different sub-modes overlap, and some sub-modes may only occur under very critical conditions, implying such sub-mode may not appear in practical applications. For example, initial conditions for sub-mode 5ab normally overlaps with sub-mode 5ba and 5bb, which means sub-mode 5ba or 5bb has a higher chance to be initiated and sub-mode 5ab may never occur.

Simply supported boundary condition may over-estimate structural response, but it is safe for design procedure. Full clamped boundary condition for beam element was discussed in [14] and the conclusion is compliant for slab in the present study. For other types of boundary

conditions with the combination of fixed, simply supported and free edge, the governing equations and failure modes will change accordingly. Future work is needed to include the boundary effects for more comprehensive understanding and wider application.

4. An application example

To demonstrate the applicability of the developed P-I diagrams, a case study is given for a structure under free air explosion. In a typical RC structure, the slab is made up of laced reinforced concrete with stirrups to increase its shear and bending strength. The transverse reinforcement ratio is 0.47 percent. Details of such blast design can be referred to UFC-3-340-02 manual [4], and are omitted here. The RC slab is simply supported at four edges. Relevant parameters are given below.

Longer half edge length: $L_a = 3$ m

Shorter half edge length: $L_b = 1.71$ m

Aspect ratio: $\eta = 1.75$

Thickness: $h = 0.2$ m

Unit square mass: $m = 500$ kg

Shear strength: $Q_0 = 175.5$ kN

Bending strength: $M_0 = 127.7$ kN·m

Charge weight: $W = 125$ kg

Once R, the normal distance from charge center to the slab, is determined, the peak reflected pressure p_0 and the duration t_d can be obtained by the charts in [4]. Subsequently, normalized pressure and impulse can be calculated. In the present case study, we took three different standoff distances, i.e., R=22.00 m, 18.01 m and 14.75 m, respectively (see Table 4).

Table 4 Case study

Point	Distance R	Duration t_d	Scaled Distance Z	Normalized Impulse I^*	Pressure p_0	Normalized Pressure P^*
Z1	22.00 m	17.98ms	4.400	0.122	0.090MPa	1.026
Z2	18.01 m	16.94ms	3.603	0.178	0.139MPa	1.584
Z3	14.75 m	15.93ms	2.950	0.295	0.245MPa	2.792

The strength ratio v is calculated as 1.374 according to Eq.(3), and the failure criteria in Eq. (1) with β_0 =2.5% and γ_v =1% are used. The sub-mode is mode 3ba. In Fig. 11, point Z1 is in no-damage region, point Z2 is in shear damage region, and point Z3 is in combined damage region. That means, when the scaled distance is 2.950 m/kg$^{1/3}$, the slab will suffer both shear and bending failure; when the scaled distance is 3.603 m/kg$^{1/3}$, the slab will experience shear failure only; and when the scaled distance is 4.400 m/kg$^{1/3}$, the slab is safe.
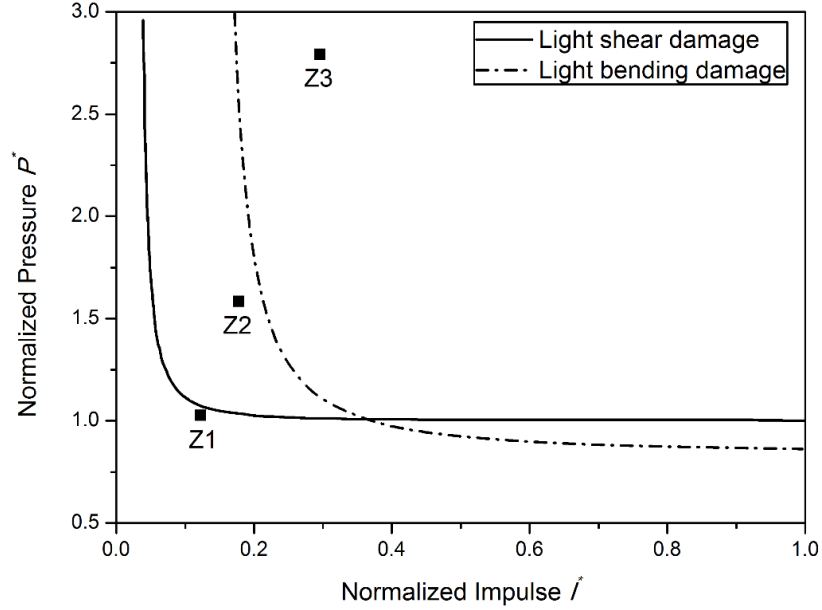

Fig. 11 Application example

5. Conclusions

This paper presents analytical solutions of slab responses subjected to blast load. The analytical solutions are derived based on a rigid-plastic slab model. A total of fourteen possible sub-modes for slab failure are considered in the theoretical derivations. Accuracy of the derived analytical solutions is verified by numerical simulation results with a numerical model validated by field blasting test data reported by other researchers.

Acknowledgement

References

[1] DoD-6055.09-STD (2008) DOD ammunition and explosives safety standards. US Department of Defense

[2] Yu JL, Jones N (1991) Further experimental investigations on the failure of clamped beams under impact loads. Int J Solids Struct 27(9):1113-1137

[3] Krauthammer T (1998) Blast mitigation technologies: developments and numerical considerations for behavior assessment and design. Proceedings of international conference on structures under shock and impact, SUSI, Melbourne, Australia: 1-10

[4] UFC-3-340-02 (2008) Structures to resist the effect of accidental explosions. US Department of the Army. Navy and Air Force Technical Manual.

[5] Li QM, Meng H (2002) Pressure-impulse diagram for blast loads based on dimensional analysis and single-degree-of-freedom model. J Eng Mech-ASCE 128(1):87-92

[6] Campidelli M, Viola E (2007) An analytical–numerical method to analyze single degree of freedom models under airblast loading. J Sound Vib 302(1–2):260-286

[7] Fallah AS, Louca LA (2007) Pressure–impulse diagrams for elastic-plastic-hardening and softening single-degree-of-freedom models subjected to blast loading. Int J Impact Eng 34(4): 823-842

[8] Krauthammer T, Bazeos N, Holmquist T (1986) Modified SDOF analysis of RC box-type structures. J Struct Eng-ASCE 112(4):726-744

[9] Low HY, Hao H (2002) Reliability analysis of direct shear and flexural failure modes of RC slabs under explosive loading. Eng Struct 24(2):189-198

[10] Martin J, Symonds PS (1965). Mode approximations for impulsively loaded rigid plastic structures, DTIC Document.

[11] Jones N, Jones C (2002) Inelastic failure of fully clamped beams and circular plates under impact loading. Proc Inst Mech Eng C-J Mech E 216(2):133-149

[12] Li QM, Jones N (1999) Shear and adiabatic shear failures in an impulsively loaded fully clamped beam. Int J Impact Eng 22(6):589-607

[13] Symond PS, Chon CT (1979) Large viscoplastic deflections of impulsively loaded plane frames. Int J Solids Struct 15(1):15-31

[14] Ma GW, Shi HJ, Shu DW (2007) P-I diagram method for combined failure modes of rigid-plastic beams. Int J Impact Eng 34(6):1081-1094

[15] Ma GW, Huang X, Li JC (2010) Simplified Damage Assessment Method for Buried Structures against External Blast Load. J Struct Eng-ASCE 136(5):603-612

[16] Huang X, Ma G, Li J (2010) Damage assessment of reinforced concrete structural elements subjected to blast load. Int J Protect Struct 1(1):103-124

[17] Huang X, He L, Ma GW (2011) Soil-Structure Interaction and Pulse Shape Effect on Structural Element Damage to Blast Load. J Perform Constr Facil 25(5):400-410

[18] Huang X (2011) Damage assessment of structures against blast load based on mode approximation method. PhD thesis, Nanyang Technological University

[19] Yuen SCK, Nurick GN (2005) Experimental and numerical studies on the response of quadrangular stiffened plates. Part I: Subjected to uniform blast load. Int J Impact Eng

31(1):55-83

[20] Balden VH, Nurick GN (2005) Numerical simulation of the post-failure motion of steel plates subjected to blast loading. Int J Impact Eng 32(1-4):14-34

[21] Bonorchis D, Nurick GN (2010) The analysis and simulation of welded stiffener plates subjected to localised blast loading. Int J Impact Eng 37(3):260-273

[22] Kumar P, LeBlanc J, Stargel DS, Shukla A (2012) Effect of plate curvature on blast response of aluminum panels. Int J Impact Eng 46:74-85

[23] Li X, Wang ZH, Zhu F, Wu GY, Zhao LM (2014) Response of aluminium corrugated sandwich panels under air blast loadings: Experiment and numerical simulation. Int J Impact Eng 65:79-88

[24] Rajendran R, Lee JM (2009) Blast loaded plates. Mar Struct 22(2):99-127

[25] Nurick GN, Gelman ME, Marshall NS (1996) Tearing of blast loaded plates with clamped boundary conditions. Int J Impact Eng 18(7–8):803-827

[26] Nurick GN, Shave GC (1996) The deformation and tearing of thin square plates subjected to impulsive loads—An experimental study. Int J Impact Eng 18(1):99-116

[27] Bai YL, Johnson W (1982) Plugging: physical understanding and energy absorption. Met Technol 9(1):182-190

[28] Li QM, Jones N (2000) Formation of a shear localization in structural elements under transverse dynamic loads. Int J Solids Struct 37(45):6683-6704

[29] Youngdahl CK (1970) Correlation Parameters for Eliminating the Effect of Pulse Shape on Dynamic Plastic Deformation. J Appl Mech 37(3):744-752

[30] Youngdahl CK (1971) Influence of pulse shape on the final plastic deformation of a circular plate. Int J Solids Struct 7(9):1127-1142

[31] Li QM, Meng H (2002) Pulse loading shape effects on pressure–impulse diagram of an elastic–plastic, single-degree-of-freedom structural model. Int J Mech Sci 44(9):1985-1998

[32] Li QM, Jones N (2005) Foundation of correlation parameters for eliminating pulse shape effects on dynamic plastic response of structures. J Appl Mech 72(2):172-176

[33] Jones J, Wu C, Oehlers DJ, Whittaker AS, Sun W, Marks S, Coppola R (2009) Finite difference analysis of simply supported RC slabs for blast loadings. Eng Struct 31(12):2825-2832